Observing algebraic variety of Lee-Yang zeros in asymmetrical systems via a quantum probe

Arijit Chatterjee [1,*] T. S. Mahesh,[1,†] Mounir Nisse,[2,‡] and Yen-Kheng Lim[2,§]

[1]*Department of Physics and NMR Research Center, Indian Institute of Science Education and Research, Pune, India*
[2]*School of Mathematics and Physics, Xiamen University Malaysia, 43900 Sepang, Malaysia*

Lee-Yang (LY) zeros, points on the complex plane of physical parameters where the partition function goes to zero, have found diverse applications across multiple disciplines like statistical physics, protein folding, percolation, and complex networks. However, experimental extraction of the complete set of LY zeros for general asymmetrical classical systems remains a crucial challenge to put those applications into practice. Here, we propose a qubit-based method to simulate an asymmetrical classical Ising system, enabling the exploration of LY zeros at arbitrary values of physical parameters like temperature and internal couplings. Without assuming system symmetry, the full set of LY zeros forms an algebraic variety in a higher-dimensional complex plane. To determine this variety, we project it into sets representing magnitudes (amoeba) and phases (coamoeba) of LY zeros. Our approach uses a probe qubit to initialize the system and to extract LY zeros without assuming any control over the system qubits. This is particularly important as controlling system qubits can get intractable with the increasing complexity of the system. Initializing the system at an amoeba point, coamoeba points are sampled by measuring probe qubit dynamics. Iterative sampling yields the entire algebraic variety. Experimental demonstration of the protocol is achieved through a three-qubit NMR register. This paper expands the horizon of quantum simulation to domains where identifying LY zeros in general classical systems is pivotal. Moreover, by extracting abstract mathematical objects like amoeba and coamoeba for a given polynomial, our paper integrates pure mathematical concepts into the realm of quantum simulations.

I. INTRODUCTION

It is commonly understood that complex numbers merely play the role of a calculational tool in physics, while observable quantities are represented by real numbers. In 1952, Lee and Yang published two landmark papers [1,2] showing the partition function of a system can become zero at certain points on the complex plane of its physical parameters. These zeros, now known as Lee-Yang (LY) zeros, provide a cohesive understanding of equilibrium phase transition [3] as they correspond to the nonanalyticity of free energies. However, it was widely believed that LY zeros cannot be observed directly as they occur at complex values of physical parameters, and only when they approach the real axis their presence gets disclosed as the system goes through a phase transition.

Nevertheless, this does not mean that complex LY zeros have nothing to say about the physical system. In fact, determination of LY zeros can play a key role in studying the thermodynamic behavior of complicated many-body systems as they fully characterize the partition function. Apart from that, recent studies [4,5] have paved the way for determining universal critical exponents of phase transitions from LY zeros, which is otherwise a computationally difficult

problem due to critical slowdown. It was also observed that LY zeros can be employed to understand nonequilibrium phenomena like dynamical phase transitions [6], along with other statistical studies [7,8] like percolation [9] or complex networks [10,11] and even protein folding [12,13]. Profound links between thermodynamics in the complex plane and dynamical properties of quantum systems have also been discovered [14–18] in recent years. All these discoveries have made the determination of LY zeros for general classical systems a crucial necessity in various disciplines of physics.

In 2012, by representing a classical Ising chain with a small number of spins, Wei and Liu showed [19] that the complex LY zeros for such a system can be mapped to the zeros of quantum coherence of an interacting probe. Using this method, the experimental observation of LY zeros was directly achieved [20].

This opens up the possibility of using quantum simulation techniques to simulate classical systems and determine their LY zeros with a quantum probe, as demanded in many areas of physics. However, there are two major challenges to overcome. First of all, the method proposed in [19] and successive experiments [4,20] reported observation of LY zeros lying on a single complex plane $\mathbb{C}$. This happens when the partition function is expandable as a univariate polynomial, known as the LY polynomial, in terms of the complexified physical parameter. This condition of the LY polynomial being univariate is based on a symmetry assumption about the system. For example, in the case of the Ising chain, it assumes that all the spins will experience the same local

*chatterjee.arijit@students.iiserpune.ac.in
†mahesh.ts@iiserpune.ac.in
‡mounir.nisse@gmail.com, mounir.nisse@xmu.edu.my
§yenkheng.lim@gmail.com, yenkheng.lim@xmu.edu.my

(complexified) magnetic field. Unfortunately, a general system will not necessarily have this symmetry. Thus, the partition function, in general, is to be expanded as a multivariate LY polynomial in terms of complexified parameters. In the worst case, an N spin Ising chain will have an N variate LY polynomial if all the spins experience different local fields. In such a scenario, LY zeros of the system will form an algebraic variety [21] $V \subset (\mathbb{C}^*)^N$, where $\mathbb{C}^* = \mathbb{C} - \{0\}$. Therefore, finding a method to experimentally determine the full algebraic variety containing LY zeros of a general asymmetrical system is crucial. The second challenge to overcome is that a quantum simulator of the classical system should have ways to simulate the system at a wide range of its physical parameters like temperature and internal couplings. This flexibility in initialization is crucial to uncover the full set of LY zeros corresponding to all physical situations. However, the systems under study can get complicated and thus achieving full quantum control over system qubits can get challenging. Therefore, the desired method should not assume much experimental control over the system qubits so that it can be extended to complex systems in the future.

In this paper, we show the direct experimental determination of the algebraic variety containing roots of a general multivariate LY polynomial for asymmetrical Ising-type systems. Mathematical developments in the last few decades unveil that one can project the algebraic variety to sets of coordinatewise absolute values and arguments, called the amoeba [22,23] and coamoeba [24–27], respectively. More precisely, we consider in this paper a polynomial of two complex variables, $f(z_1, z_2)$. The set of values (z_1, z_2) which make $f(z_1, z_2) = 0$ is what we call the algebraic variety, which is a three-(real)-dimensional object living in (four-real-dimensional) complex space $(\mathbb{C}^*)^2$. The amoeba is obtained by taking logarithms of their absolute values $(\ln |z_1|, \ln |z_2|)$ of the variety, and the coamoeba is obtained by taking its arguments $(\arg z_1, \arg z_2)$. In this sense, the abstract variety living in a higher-dimensional complex space is studied by projecting into domains of lower-dimensional real spaces.

We use qubits to simulate the classical asymmetrical Ising system which can be controlled through another qubit acting as a probe. We highlight that, like an ideal quantum simulator, the system can be simulated at any arbitrary point on its amoeba at any arbitrary temperature. Even the internal coupling of the Ising system can be set to a desired value ranging from ferromagnetic to antiferromagnetic regimes. This initialization is accomplished solely by manipulating the probe qubit, leaving the system qubits undisturbed. After effectively initiating the system at an arbitrarily chosen point on its amoeba, corresponding points of coamoeba can be directly sampled from the time evolution of the probe's coherence. By iterating the process, one samples the coamoeba across the amoeba to obtain the full algebraic variety. Thus both preparation and detection are achieved through the probe alone. We demonstrate the method experimentally via a three-qubit NMR register by taking two of them as system and the third one as probe. Sampling of coamoeba at different points on amoeba is performed directly from the time domain NMR signal without any need for extensive postprocessing of experimental data. Apart from extending the range of quantum simulations to other areas of physics where determining

LY zeros of general classical system is pivotal, our paper also brings pure mathematical structures like amoeba and coamoeba into the realm of quantum simulations by physically sampling them for a given LY polynomial.

The rest of the paper is organized as follows. In Sec. II, we introduce the asymmetric Ising system and show how to use qubits as system and probe such that the amoeba and the coamoeba of the algebraic variety corresponding to the LY polynomial of the system relate to the probe qubit's coherence. After describing the methodology of sampling the algebraic variety in Sec. III, we discuss how to initialize the system qubits at any desired point on the amoeba at any value of physical parameters like temperature and coupling constant by operating on only the probe in Sec. IV. Finally, we present the experimental results in Sec. V before concluding in Sec. VI.

II. TWO-SPIN ISING MODEL AND (CO)AMOEBAS

To explain the method, we consider our system to be a classical Ising chain consisting of only two sites, A and B, coupled to each other with strength J. Without assuming any symmetry, let the magnetic fields at sites A and B be h_A and h_B, respectively. This classical system can be mimicked by using two spin-1/2 systems as qubits with Hamiltonian $H_{AB} = -J\sigma_z^A \sigma_z^B - h_A \sigma_z^A - h_B \sigma_z^B$, where σ_i^X is the Pauli i operator of spin X.

In a thermal bath of inverse temperature β, the partition function of AB is

$$Z(\beta, h_A, h_B) = e^{\beta J + \beta h_A + \beta h_B} \big(1 + e^{-2\beta J - 2\beta h_A} \\ + e^{-2\beta J - 2\beta h_B} + e^{-2\beta h_A - 2\beta h_B} \big). \quad (1)$$

We extend Z into the complex domain by letting

$$e^{-2\beta h_A} = z_1, \quad e^{-2\beta h_B} = z_2, \quad \text{where } (z_1, z_2) \in (\mathbb{C}^*)^2. \quad (2)$$

Further, by identifying $\Gamma = e^{-2\beta J} \in \mathbb{R}_+$, the partition function becomes $Z = (\Gamma z_1 z_2)^{-1/2} f(z_1, z_2)$, where

$$f(z_1, z_2) = 1 + \Gamma z_1 + \Gamma z_2 + z_1 z_2 \quad (3)$$

is the two-spin bivariate LY polynomial. Zeros of the partition function now correspond to the vanishing of this polynomial, which defines the algebraic variety $V_f = \{(z_1, z_2) \in (\mathbb{C}^*)^2 \mid f(z_1, z_2) = 0\}$.

For any complex number (z_1, z_2) lying on V_f, information about its absolute value is studied using a log map $\log : (\mathbb{C}^*)^2 \to \mathbb{R}^2$ by taking $(z_1, z_2) \mapsto (\ln |z_1|, \ln |z_2|)$. The image $\mathcal{A}_f = \log(V_f)$ is called the amoeba. On the other hand, information about the phase is studied using the argument map $\arg : (\mathbb{C}^*)^2 \to S^1 \times S^1$ where $(z_1, z_2) \mapsto (\arg z_1, \arg z_2)$. The image $\text{co}\mathcal{A}_f = \arg(V_f)$ is called the coamoeba. For example, the amoeba and coamoeba for $\Gamma = \frac{1}{2}$ in Eq. (3) are shown in Fig. 1.

To observe these complex zeros, we adopt the procedure of Wei and Liu [19] by introducing another spin-1/2 particle, which acts as a quantum probe. Its states $\{|0\rangle, |1\rangle\}$ (here $|0\rangle$ and $|1\rangle$ are eigenvectors of σ_z with eigenvalues ± 1, respectively) span a two-dimensional Hilbert space $\mathcal{H}_P$. The total space is now $\mathcal{H}_{\text{tot}} = \mathcal{H}_P \otimes \mathcal{H}_{AB}$. However, here we allow the probe to couple asymmetrically with A and B. This is because,
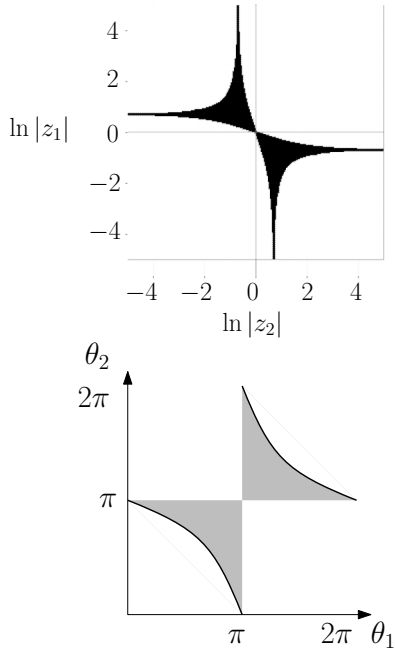
FIG. 1. The amoeba (top) and coamoeba (bottom) of the LY polynomial $f(z_1, z_2) = 1 + \frac{1}{2}z_1 + \frac{1}{2}z_2 + z_1 z_2$ [28].

in our case, h_A and h_B are not necessarily equal, and hence z_1 and z_2 must be distinct variables, necessitating the description of Lee-Yang zeros in $(\mathbb{C}^*)^2$ rather than in $\mathbb{C}$.

Suppose that the probe spin σ_z^P couples to σ_z^A and σ_z^B with coupling strengths λ_A and λ_B, respectively. This situation is depicted in Fig. 2(a). The interaction Hamiltonian is

$$H_{\text{int}} = \lambda_A \sigma_z^P \sigma_z^A + \lambda_B \sigma_z^P \sigma_z^B. \tag{4}$$

Here we used the notation $\sigma_z^P \sigma_z^A = \sigma_z^P \otimes \sigma_z^A \otimes \mathbb{1}$ and $\sigma_z^P \sigma_z^B = \sigma_z^P \otimes \mathbb{1} \otimes \sigma_z^B$. The full Hamiltonian now becomes $H = \mathbb{1} \otimes H_{AB} + H_{\text{int}}$, or

$$H = -J\sigma_z^A \sigma_z^B - (h_A - \lambda_A \sigma_z^P)\sigma_z^A - (h_B - \lambda_B \sigma_z^P)\sigma_z^B. \tag{5}$$

The full initial state at time $t = 0$ is taken to be

$$\rho(0) = |\psi_P\rangle\langle\psi_P| \otimes \frac{\exp(-\beta H_{AB})}{Z(\beta, h_A, h_B)}, \tag{6}$$
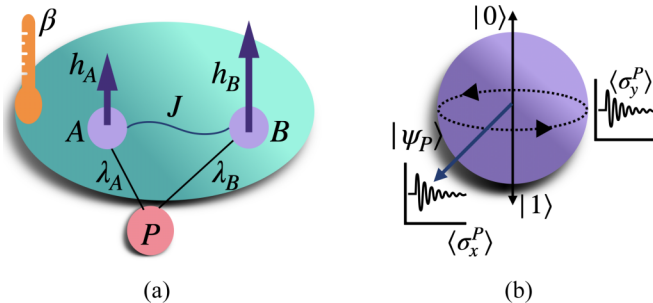

(a)

(b)

FIG. 2. (a) A two-spin Ising system in a thermal bath at temperature $1/\beta$ coupled to a probe spin. (b) As the probe evolves under the interaction with the system, its coherence is recorded by measuring $\langle\sigma_x^P\rangle$ and $\langle\sigma_y^P\rangle$ with time.

where $|\psi_P\rangle$ is a pure coherent quantum state in the probe's σ_z basis. Here, by a coherent state we mean that $|\psi_P\rangle$ has superposition in $\{|0\rangle, |1\rangle\}$ basis. It subsequently evolves under the Hamiltonian in Eq. (5) as $\rho(t) = \mathcal{U}(t)\rho(0)\mathcal{U}^\dagger(t)$, where $\mathcal{U}(t) = e^{-itH/\hbar}$. As we only observe the evolution of the probe, we trace out AB to get $\rho_P(t) = \text{tr}_{AB}\rho(t)$. Under this evolution, the coherence L of the probe at time t can be shown to take the form

$$L(t) = \frac{\hbar^2}{4}\left|\langle\sigma_x^P(t)\rangle + i\langle\sigma_y^P(t)\rangle\right|^2 = \mathcal{C}|f(z_1, z_2)|^2, \tag{7}$$

the derivation of which can be found in Appendix A. Here $\mathcal{C}$ is a constant over time and $f(z_1, z_2)$ is the two-spin bivariate LY polynomial of Eq. (3), after identifying

$$z_1 = \exp(-2\beta h_A + 4i\lambda_A t/\hbar),$$
$$z_2 = \exp(-2\beta h_B + 4i\lambda_B t/\hbar), \text{ and}$$
$$\Gamma = \exp(-2\beta J). \tag{8}$$

Note that the variables z_1 and z_2 become complex as the time evolution introduces a complex phase. Furthermore, we note

$$\ln|z_1| = -2\beta h_A, \quad \ln|z_2| = -2\beta h_B, \text{ and} \tag{9a}$$

$$\theta_1(t) = \arg z_1 = \frac{4\lambda_A t}{\hbar}, \quad \theta_2(t) = \arg z_2 = \frac{4\lambda_B t}{\hbar}. \tag{9b}$$

Corresponding to the set of points $\{(z_1, z_2)\}$ for which $|f(z_1, z_2)|^2 = 0$, the set $\{(\ln|z_1|, \ln|z_2|)\}$ forms the amoeba while the set $\{(\arg z_1, \arg z_2)\}$ forms the coamoeba.

III. METHOD FOR OBSERVING THE ALGEBRAIC VARIETY

Our method for determining the algebraic variety V_f works as follows: we first initiate the system in the state given by Eq. (6) at arbitrary values of βh_A and βh_B, which according to Eq. (9a) fix a point on the amoeba space. As we shall see later, the preparation is achieved through the probe, assuming no control over the system qubits. Next, we let the probe interact with the system and observe its coherence. If the coherence is nonzero at all finite times, we conclude that there are no LY zeros at that value of $(\beta h_A, \beta h_B)$; hence, the chosen point does not belong to the amoeba. On the other hand, if we find the coherence vanishing at time instants $\{t_i\}$, the point $(\beta h_A, \beta h_B) \equiv (\ln|z_1|, \ln|z_2|)$ belongs to the amoeba. Moreover, by Eq. (9b), $\{t_i\}$ can be mapped to $\{(\theta_1(t_i), \theta_2(t_i))\}$, which lie on a $S^1 \times S^1$ torus as the points of the coamoeba, corresponding to the point $(\ln|z_1|, \ln|z_2|)$ on the amoeba. Upon multiple iterations of this procedure, one can sample the coamoeba across the amoeba to extract the full V_f for the multivariate LY polynomial. For more details regarding the sampling of coamoeba, see Appendix B.

Another way of seeing the fact that complex LY zeros leave a footprint in the real-time dynamics of the probe would be in terms of correlation. Mutual information [29] between the probe and the system qubits captures the total correlation between them and is defined as

$$I_{P:AB}(t) = S_P(t) + S_{AB}(t) - S_{PAB}(t), \tag{10}$$

where $S_X(t) = -\text{tr}[\rho_X(t)\ln\rho_X(t)]$ is the von Neumann entropy [29] of X at time t. By evolving the initial state of Eq. (6)
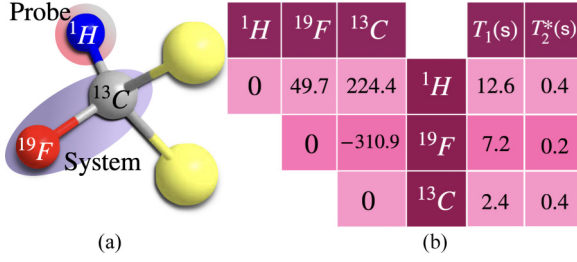
FIG. 3. (a) The molecular structure of DBFM with labeled spins. (b) Values of NMR Hamiltonian parameters (resonance offsets in diagonal and coupling constants J_{ij} in off-diagonal elements, in Hz) along with relaxation time constants.

under the Hamiltonian of Eq. (5), it can be seen that S_{AB} and S_{PAB} do not evolve over time. Therefore, according to Eq. (10), $I_{P:AB}$ becomes maximum at times only when the probe is maximally mixed, i.e., $\rho_P = \mathbb{1}/2$. The reduced density matrix of the probe can be expanded in Pauli basis as

$$\rho_P(t) = \frac{1}{2}\left(\mathbb{1} + \sum_{i\in\{x,y,z\}} c_i(t)\sigma_i^P\right), \tag{11}$$

where $c_i(t) = \langle \sigma_i^P(t)\rangle$. It can be easily seen that $\partial_t c_z = 0$ in the evolution under the Hamiltonian of Eq. (5). If the initial state of the probe is such that $c_z(0) = 0$, then its reduced density matrix becomes maximally mixed at time points where $\langle \sigma_x^P\rangle$ and $\langle \sigma_y^P\rangle$ simultaneously vanish, i.e., points corresponding to LY zeros. Therefore, only at the time points corresponding to LY zeros, the correlation between the probe and the system becomes maximum.

IV. SYSTEM INITIALIZATION VIA A QUANTUM PROBE

A. NMR register

For a concrete demonstration via NMR, we use a liquid ensemble of three spin-1/2 (three-qubit) nuclear registers of ^{13}C-dibromofluoromethane (DBFM) [see Fig. 3(a)], dissolved in acetone-D6, by identifying ^{1}H as probe P and ^{19}F and ^{13}C as system spins A and B, respectively. In a high static magnetic field of $B_0 = 11.7$ T, their Larmor frequencies have magnitudes $\omega_i = \gamma_i B_0$, where γ_i are the gyromagnetic ratios [30]. The three spins also interact mutually via scalar coupling with strengths J_{ij} as tabled in Fig. 3(b). In terms of the spin operators $I_\alpha^i = \sigma_\alpha^i/2$, the laboratory-frame NMR Hamiltonian is of the form $H_{\text{NMR}} = H_I + H_{\text{rf}}$, with internal part $H_I = -\sum_i \hbar\omega_i I_z^i + 2\pi\hbar\sum_{i\neq j} J_{ij} I_z^i I_z^j$ and the probe control part $H_{\text{rf}} = -\hbar\Omega_P(t)I_x^P$. Here $\Omega_P(t) = \gamma_i B_P(t)$ represents the control amplitude achieved through the magnetic component $B_P(t)$ of the applied circularly polarized rf field resonant with the probe's Larmor frequency. Notice, the control Hamiltonian contains only the probe's component $\Omega_P(t)$, while we set $\Omega_A(t) = \Omega_B(t) = 0$ to ensure that the method works without assuming any experimental control over the system.

We allow the liquid ensemble register to equilibrate at an ambient temperature of $T = 300$ K inside a 500-MHz Bruker NMR spectrometer. As $\hbar\omega_i \ll k_B T$, the density operator in the thermal state becomes $\rho_{\text{th}} = \exp(-\beta H_I)/\text{tr}[\exp(-\beta H_I)] \approx \mathbb{1}/8 + \epsilon\rho_{\text{th}}^\Delta$, where $\rho_{\text{th}}^\Delta = I_z^H + (\gamma_F/\gamma_H)I_z^F + (\gamma_C/\gamma_H)I_z^C$ is the

deviation thermal state and the purity factor $\epsilon \approx 10^{-5}$. From the thermal state, preparation of the initial state in Eq. (6) at any chosen values of $\{\beta h_A, \beta h_B\}$ is to be achieved, subject to the constraint that the system (^{19}F, ^{13}C) remains inaccessible. From now onward the probe's state of Eq. (6) is taken to be $|\psi_P\rangle = (|0\rangle + |1\rangle)/\sqrt{2}$.

B. Initializing at the origin of the amoeba plane

First consider the preparation for $h_A = h_B = 0$, which corresponds to the origin of amoeba in accordance to Eq. (9a). We note that the factor $\exp(-\beta H_{AB})$ of Eq. (6) can be expanded as

$$e^{-\beta H_{AB}} = e^{\beta J\sigma_z^A\sigma_z^B}e^{\beta h_A\sigma_z^A}e^{\beta h_B\sigma_z^B}$$

$$= C_a\mathbb{1}_4 + C_b\sigma_z^A + C_c\sigma_z^B + C_d\sigma_z^A\sigma_z^B,$$

$$\text{where } C_a = [\cosh(\beta J)\cosh(\beta h_A)\cosh(\beta h_B)$$
$$+ \sinh(\beta J)\sinh(\beta h_A)\sinh(\beta h_B)],$$
$$C_b = [\cosh(\beta J)\sinh(\beta h_A)\cosh(\beta h_B)$$
$$+ \sinh(\beta J)\cosh(\beta h_A)\sinh(\beta h_B)],$$
$$C_c = [\cosh(\beta J)\cosh(\beta h_A)\sinh(\beta h_B)$$
$$+ \sinh(\beta J)\sinh(\beta h_A)\cosh(\beta h_B)],$$
$$C_d = [\cosh(\beta J)\sinh(\beta h_A)\sinh(\beta h_B)$$
$$+ \sinh(\beta J)\cosh(\beta h_A)\cosh(\beta h_B)]. \tag{12}$$

Substituting the above to Eq. (6) and setting $h_A = h_B = 0$, the initial state in this case becomes $\rho(0) = \mathbb{1}/8 + (1/2)\tanh(\beta J)I_z^A I_z^B + [\cosh(\beta J)I_x^P + \sinh(\beta J)4I_x^P I_z^A I_z^B]/Z(\beta, 0, 0)$. Here the first two terms can be suppressed as they remain invariant under time evolution governed by H_I, and also do not contribute to the probe's coherence in Eq. (7). Therefore, the target state for initialization reads

$$\rho^\Delta(0) = \left[\cosh(\beta J)I_x^P + \sinh(\beta J)4I_x^P I_z^A I_z^B\right]/Z(\beta, 0, 0), \tag{13}$$

where Δ is used as a superscript to indicate that redundant terms are suppressed as mentioned earlier. For the same reason we ignore the identity term of ρ_{th} and consider only the deviation thermal state ρ_{th}^Δ. We have to realize the target initial state $\rho^\Delta(0)$ of Eq. (13) from the deviation thermal state ρ_{th}^Δ. In other words, for initialization, the target state of Eq. (13) is to be achieved starting from $\rho_{\text{th}}^\Delta(0)$ with the constraint that the system remains inaccessible. For this purpose, we employ the pulse sequence shown in Fig. 4(a) which operates on the probe spin of ^{1}H only. Detailed derivation of the pulse sequence is given in Appendix C 1. Here, the delay time τ of the pulse sequence is a free parameter that depends directly on the value of $\beta J \in \mathbb{R}$ of the target state as $\exp(\beta J) = \cos[\pi(J_{PA} + J_{PB})\tau]/\cos[\pi(J_{PA} - J_{PB})\tau]$. This direct dependency allows us to initiate the system at any value of βJ in both ferromagnetic ($\beta J \in \mathbb{R}_+$) and antiferromagnetic ($\beta J \in \mathbb{R}_-$) regimes just by varying the delay τ suitably, as discussed in detail in Appendix C 1.

C. Initialization on nonorigin points of the amoeba plane

To sample coamoeba corresponding to nonorigin points on amoeba, we need h_A and h_B to take nonzero values. The state
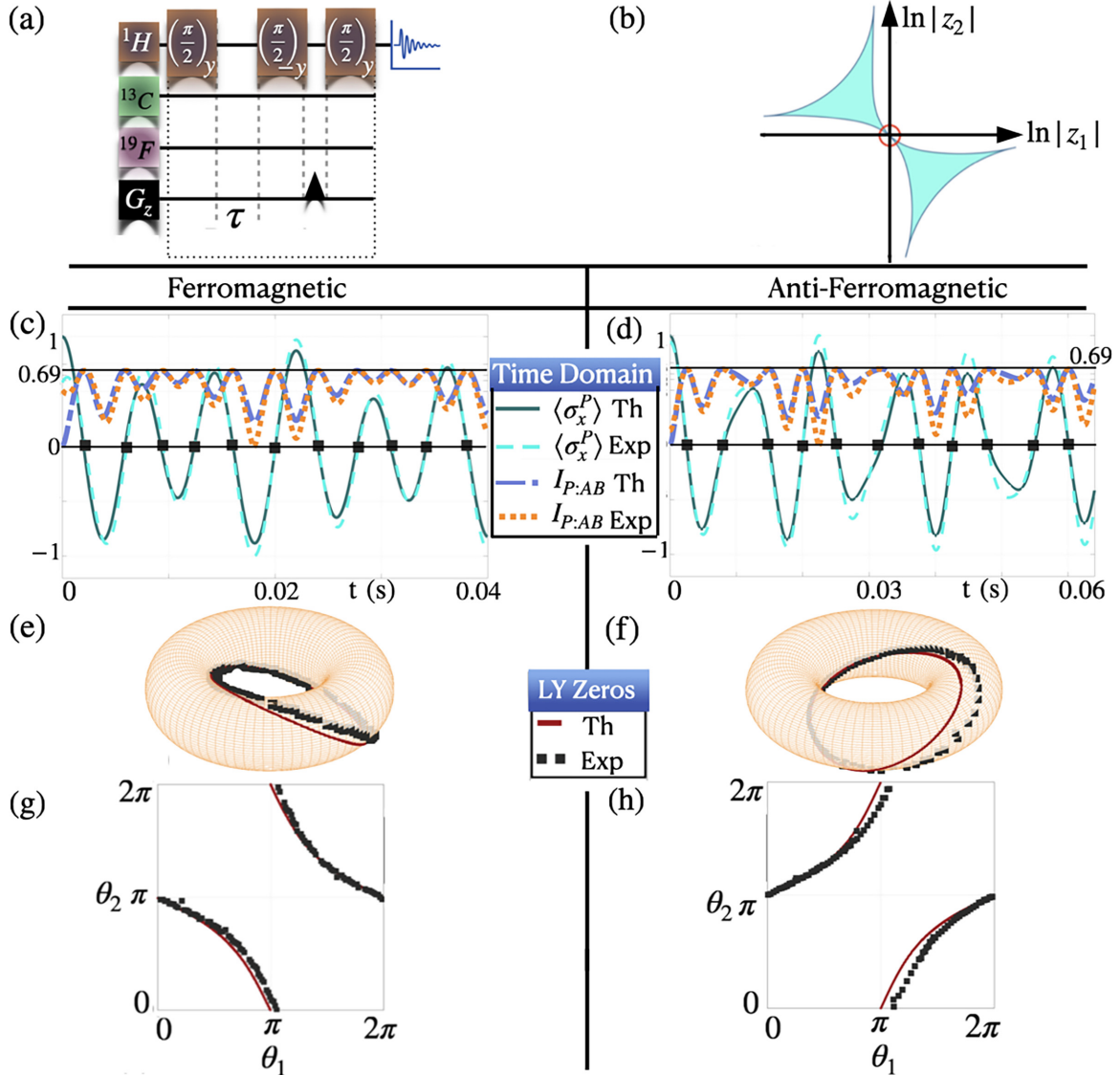
FIG. 4. (a) Pulse sequence for preparing the system in the state of Eq. (6) for $h_A = h_B = 0$. We set $\tau = 8.76$ or 9.013 ms to prepare $\beta J = 0.5$ (ferromagnetic case) or -0.5 (antiferromagnetic case) respectively. The corresponding amoeba point is at the origin of the complex plane as illustrated in (b). (c), (d) The real parts of FID (dashed lines) corresponding to $\langle \sigma_x^P(t) \rangle$ are plotted along with the simulated curves (solid lines) for (c) ferromagnetic and (d) antiferromagnetic cases respectively. As $\langle \sigma_y^P(t) \rangle$ is identically zero in these cases, the FID null points (solid squares) correspond to LY zeros. Theoretical and experimental values of the mutual information $I_{P:AB}$ between the probe and the system are also plotted, which reach their maxima (horizontal line at 0.69) only at the LY zeros. (e), (f) Theoretically calculated (solid line) and experimentally observed (filled squares) coamoeba on a 2-torus for (e) ferromagnetic and (f) antiferromagnetic cases respectively. (g), (h) Corresponding planar visualizations.

of Eq. (6) can be directly computed as $\rho(0) = (\mathbb{1}/2 + I_x^P) \otimes (e^{-\beta H_{AB}}/Z(\beta J, h_A, h_B))$, which, upon substituting the value of $e^{-\beta H_{AB}}$ from Eq. (12), yields

$$\rho^{\Delta}(0) = C_a I_x^P + C_b 2I_x^P I_z^A + C_c 2I_x^P I_z^B + C_d 4I_x^P I_z^A I_z^B. \quad (14)$$

Here, we have used "tilde" as before to indicate that only those terms that contribute to the probe's coherence are considered whereas $\mathbb{1}$ and $I_z^A I_z^B$ are suppressed. C_i of Eq. (14) are hyperbolic functions of βh_A, βh_B, and βJ as defined in Eq. (12). Again, starting from the thermal deviation ρ_{th}^{Δ}, target state $\rho^{\Delta}(0)$ of Eq. (14) can be prepared with only probe control using the pulse sequence shown in Fig. 5(a). The derivation of pulse sequence is given in Appendix D which explains how

the pulse sequence achieves the desired initialization. As there are three variables (βJ, βh_A, βh_B) to fix the target state of Eq. (14), the pulse sequence of Fig. 5(a) is also having three free parameters θ^1, θ^2, and τ, which can be set suitably to prepare any desired state. Given a specific target state, how to obtain the correct values of three control parameters θ^1, θ^2, and τ is discussed in Appendix D.

V. EXPERIMENTAL RESULTS

As explained above, LY zeros are extracted from the time points where probe coherence vanishes, which, according to Eq. (7), leads to simultaneous vanishing of $\langle \sigma_x^P \rangle$ and $\langle \sigma_y^P \rangle$.
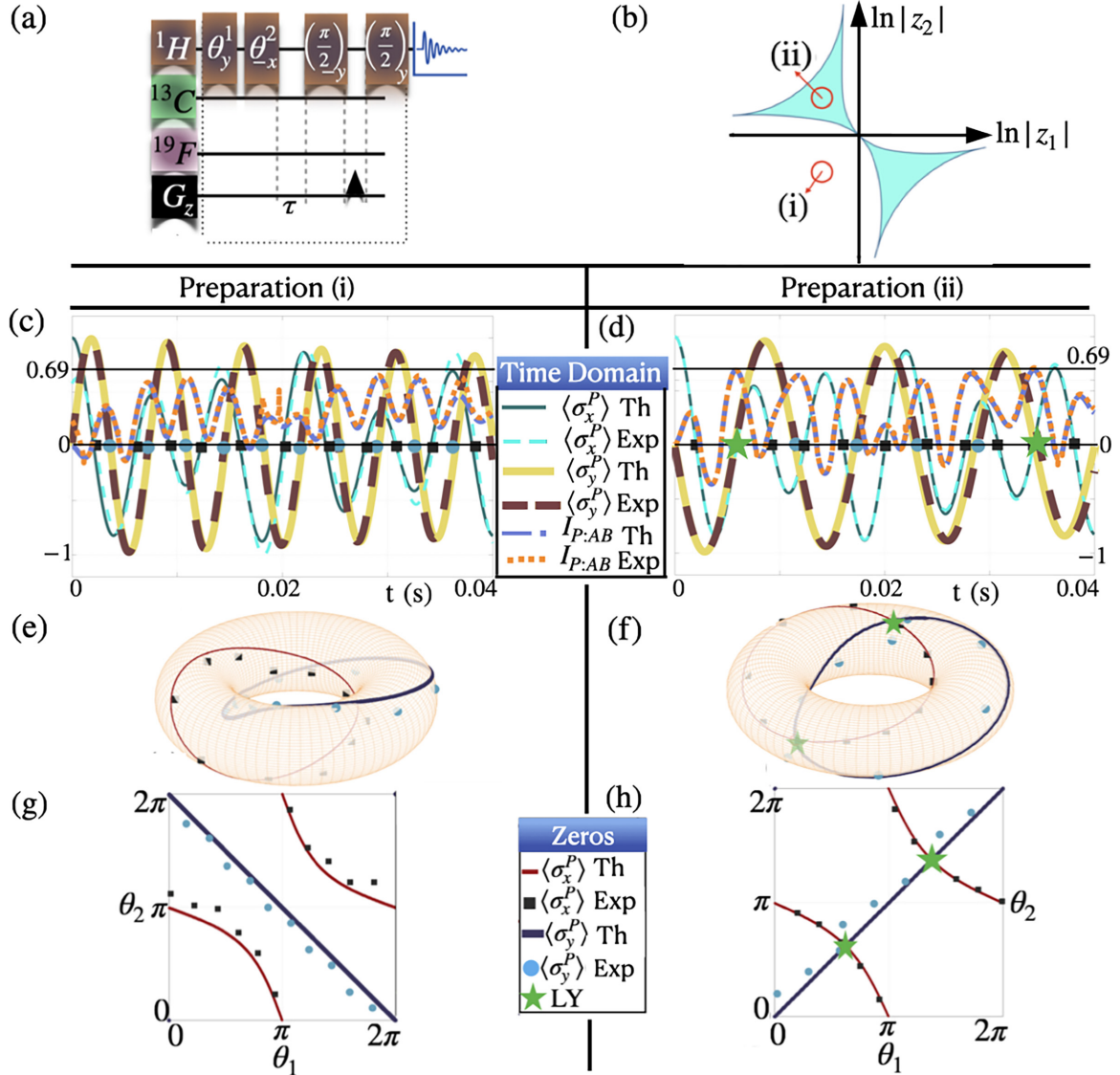
FIG. 5. (a) Pulse sequence for preparing the system in the state of Eq. (6) for nonzero values of h_A and h_B. (b) In particular, the initialization is performed for two distinct points on the amoeba plane: (i) $h_A = h_B = 0.1$ and (ii) $h_A = -h_B = 0.1$, considering $\beta J = 0.5$ in both cases. (c), (d) The real parts (dashed thin lines) and imaginary parts (dashed thick lines) of FID corresponding to $\langle \sigma_x^P(t) \rangle$ and $\langle \sigma_y^P(t) \rangle$, respectively, are plotted along with the simulated curves (solid lines, thin and thick correspondingly) for the prepared initial state of (i) in (c) and (ii) in (d). Simultaneous null points of real (solid square) and imaginary (solid circle) parts of FID correspond to LY zeros, which exist for (ii) (stars) while absent for (i). Theoretical and experimental curves of the mutual information $I_{P:AB}$ between the probe and the system are also plotted, which reach their maxima (horizontal line at 0.69) only at the LY zeros. (e), (f) Theoretically calculated (solid line) and experimentally observed null points of real (solid square) and imaginary (solid circle) parts of FID are plotted on the 2-torus for (i) (e) and (ii) (f). The desired coamoeba points lie in the intersection, which can be seen in (f). (g), (h) Corresponding planar visualizations.

As the prepared state $\rho^\Delta(0)$ evolves freely under the internal Hamiltonian H_I, we measure the probe expectation values $\langle \sigma_x^P(t) \rangle$ and $\langle \sigma_y^P(t) \rangle$ in a rotating frame synchronous with the probe's Larmor precession [30,31]. In this frame, the effective Hamiltonian becomes

$$H_{\text{eff}} = 2\pi\hbar\left(J_{PA} I_z^P I_z^A + J_{PB} I_z^P I_z^B\right), \qquad (15)$$

where A-B interaction is suppressed since $\rho^\Delta(0)$ of Eq. (13) and (14) do not evolve under it. By comparing this Hamiltonian with the interaction Hamiltonian H_{int} in Eq. (4), we identify $\lambda_A = \pi J_{PA} \hbar/2$ and $\lambda_B = \pi J_{PB} \hbar/2$. Feeding this to Eq. (9b), experimentally measured time points correspond-

ing to vanishing probe coherence are directly mapped to the coamoeba torus, and thus, physical sampling of coamoeba is achieved.

First, we sample the coamoeba corresponding to the origin [circled in Fig. 4(b)] of the amoeba's plane. Following Eq. (9a), we set $h_A = h_B = 0$ and accordingly prepare $\rho^\Delta(0)$ of Eq. (13), which subsequently evolves under H_{eff}. As $\langle \sigma_y^P(t) \rangle$ is identically zero in this case (see Appendix C 1 for calculation), LY zeros are determined just by measuring $\langle \sigma_x^P(t) \rangle$ and noting the time points where it vanishes. An essential advantage of the NMR quantum testbed is, being an ensemble architecture, it directly gives $\langle \sigma_{x(y)}^P(t) \rangle$ as the

real (imaginary) part of the NMR signal known as the free induction decay (FID) [32]. Hence, after performing the initialization via a probe in ferromagnetic and antiferromagnetic regimes, we record their FIDs, whose real parts are shown in Figs. 4(c) and 4(d), respectively. In the figure, time points corresponding to LY zeros are marked with solid squares, which are readily identified as FID null points. No additional data processing is required for this purpose. We sampled the corresponding coamoeba(s) from collected FID up to 300 ms (see Appendix C 2). However, for clarity, the time domain signals for ferromagnetic and antiferromagnetic cases in Figs. 4(c) and 4(d) are shown only up to 40 and 60 ms, respectively. The mutual information $I_{P:AB}$ between the probe and the system is calculated directly from experimental FID and plotted against their simulated values in Figs. 4(c) and 4(d). It is shown that the maximum of the mutual information occurs only at the LY zeros as predicted by Eq. (10), thus confirming the footprint of complex LY zeros in real-time correlation dynamics between the system and the probe. The FID null points are mapped to the coamoeba by Eq. (9b). The sampled coamoeba for ferromagnetic ($\beta J = 0.5$) and antiferromagnetic ($\beta J = -0.5$) regimes are shown on the 2-torus in Figs. 4(e) and 4(f) respectively. Their equivalent modulo 2π planar visualizations are shown in Figs. 4(g) and 4(h), respectively. We observe a fairly good agreement with the theoretically computed coamoeba within the experimental limitations.

It is worth noting that no state tomography is needed for these experiments, and the LY zeros emerge directly from the NMR FID without further data processing. Thus, each experiment taking less than 1 s yields a dense set of LY zeros.

We now demonstrate the sampling of coamoeba for two nonorigin points: (i) $\beta h_A = \beta h_B = 0.1$, which is outside amoeba, and (ii) $\beta h_A = -\beta h_B = 0.1$, which is inside amoeba as shown in Fig. 5(b). Again we note that $\langle \sigma_x^P(t) \rangle$ and $\langle \sigma_y^P(t) \rangle$ are just real and imaginary components of the probe (^{1}H) FID. Therefore in each case, we initialize the system considering $\beta J = 0.5$ and let it evolve under H_{eff} while recording the FID as shown in Figs. 5(c) and 5(d). We extract the time points at which $\langle \sigma_x^P(t) \rangle$ and $\langle \sigma_y^P(t) \rangle$ vanish, and map them to a 2-torus via Eq. (9b). In case (i), as shown in Figs. 5(c), 5(e), and 5(g), the zeros of $\langle \sigma_x^P(t) \rangle$ and $\langle \sigma_y^P(t) \rangle$ do not intersect, indicating the absence of L-Y zeros, thereby confirming that the point (i) does not belong to the amoeba. However, in case (ii), the null points of $\langle \sigma_x^P(t) \rangle$ (real FID) and $\langle \sigma_y^P(t) \rangle$ (imaginary FID) intersect twice as marked by stars in Figs. 5(d), 5(f), and 5(h), confirming the existence of two distinct coamoeba points. The mutual information calculated from the NMR FID is plotted along with its simulated values for case (i) [(ii)] in Fig. 5(c) [Fig. 5(d)]. It reaches its maximum twice for case (ii) at times corresponding to simultaneous null points of real and imaginary components of the FID. However, as there are no simultaneous null points of real and imaginary FID in case (i), the mutual information never becomes maximum in this case. These experimental observations confirm the prediction of Eq. (10) that the correlation between the probe and the system reaches its maximum only at points corresponding to LY zeros. It is worth highlighting that the existence and nonexistence of LY zeros for case (i) and (ii), respectively, can be directly observed just by looking at quadrature NMR FID shown in Figs. 5(c) and 5(d) without any data processing.

Again, in both cases, we see a reasonably good agreement between the theoretical predictions and experimental values. This method of high-throughput extraction of LY zeros can be used for efficient sampling of coamoeba for a large set of amoeba points, thereby determining the algebraic variety V_f at any desired precision.

VI. CONCLUSION

For the continued advancement of quantum technologies in the coming years, it is imperative that their applications extend to a broader spectrum of scientific domains by addressing challenges beyond the confines of problems related to quantum physics alone. Following the spirit, we showed a method of using qubits to simulate asymmetrical classical Ising systems at any arbitrary value of its temperature and coupling constant for determining its LY zeros in a wide range of physical situations. Most importantly, in our method, both initialization and determination of LY zeros are achieved through a quantum probe interacting with the system qubits while system qubits themselves are left untouched. We believe this feature of our protocol makes it easier to generalize for more complex systems where controlling system qubits become intractable. A lot of recent works presented a wide range of applications of LY zeros in solving problems across areas like statistical studies [7,8] of equilibrium (phase transition, critical phenomena, etc. [4,5]) and nonequilibrium (dynamical phase transitions, etc. [6]), statistical physics, percolation [9], complex networks [10,11], and even protein folding [12,13]. Therefore a method for extracting full algebraic variety containing LY zeros of a general asymmetrical classical system has become essential to implement these studies in real situations. We believe our method of using quantum simulation technique with control over a single qubit alone to do the task is an important step in bringing all those different areas of physics to the sphere of quantum simulation. Experimental validation using a three-qubit NMR register demonstrates the feasibility of our protocol. It is worth noting that this protocol samples the amoeba and coamoeba for a given LY polynomial and thereby can provoke applications of quantum simulations in the domain of pure mathematics. Apart from applications, this paper also uncovers the rich aesthetic structure of the LY zeros by physically sampling the algebraic variety that contains them.

APPENDIX A: RELATION BETWEEN SPIN COHERENCE AND ZEROS OF BIVARIATE LY POLYNOMIALS

The initial state of the probe and system is given in Eq. (6). We evolve this state to get $\rho(t) = \mathcal{U}(t)\rho(0)\mathcal{U}^\dagger(t)$, where
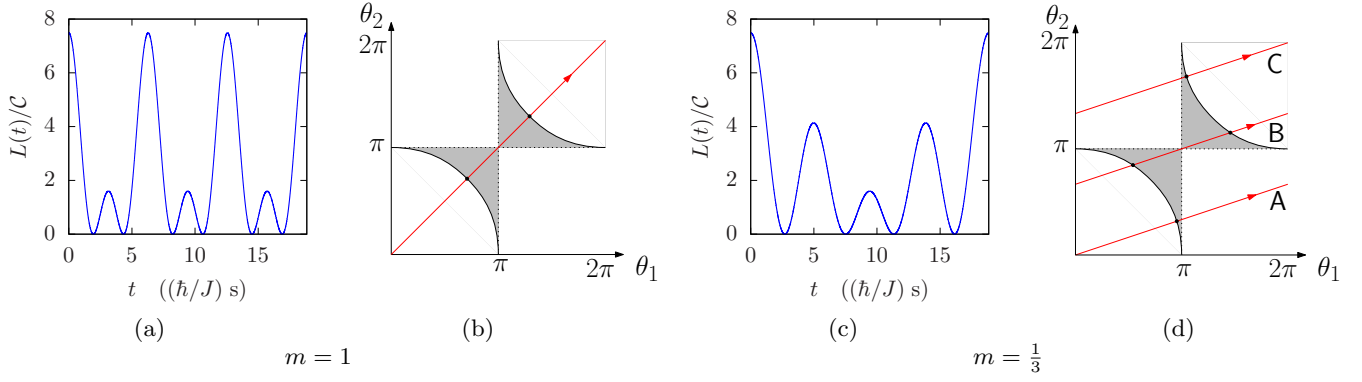
FIG. 6. The sampling of a coamoeba for $\lambda_A = J/4$, $\lambda_B = mJ/4$, and $\beta = 0.5$, for (a), (b) $m = 1$ and (c), (d) $m = \frac{1}{3}$, plotted for $0 \leqslant t \leqslant 6\pi\frac{\hbar}{J}$. (a), (c) Plots of $L(t)$ vs t. (b), (d) Parametrized lines Eq. (9b), overlaid with a sketch of the coamoeba. The points when $L(t) = 0$ correspond to the intersection of the lines with the boundary of the coamoeba.

$\mathcal{U}(t) = \exp\left(-itH/\hbar\right)$ for the Hamiltonian H given in Eq. (4):

$$\rho_P(t) = \text{tr}_{AB}(\mathcal{U}(t)\,\rho(0)\,\mathcal{U}^{\dagger}(t))$$

$$= \frac{\langle 0|\psi_P\rangle\langle\psi_P|0\rangle + \langle 1|\psi_P\rangle\langle\psi_P|1\rangle}{Z(\beta, h_A, h_B)}$$

$$+ \frac{\langle 0|\psi_P\rangle\langle\psi_P|1\rangle}{Z(\beta, h_A, h_B)}\big[e^{\beta(h_A+h_B+J)}e^{-2i(\lambda_A+\lambda_B)t/\hbar}$$

$$+ e^{\beta(h_A-h_B-J)}e^{-2i(\lambda_A-\lambda_B)t/\hbar}$$

$$+ e^{\beta(-h_A+h_B-J)}e^{-2i(-\lambda_A+\lambda_B)t/\hbar}$$

$$+ e^{\beta(-h_A-h_B+J)}e^{-2i(-\lambda_A-\lambda_B)t/\hbar}\big] + \text{H.c.}$$

From this we get (using the complexified variables z_1, z_2, and Γ defined in the main text)

$$\langle\sigma_x^P(t)\rangle = \frac{\langle 0|\psi_P\rangle\langle\psi_P|1\rangle}{Z(\beta, h_A, h_B)(\Gamma z_1 z_2)^{\frac{1}{2}}}$$

$$\times (1 + \Gamma z_1 + \Gamma z_2 + z_1 z_2) + \text{H.c.}, \quad\text{(A1)}$$

and

$$\langle\sigma_y^P(t)\rangle = i\frac{\langle 0|\psi_P\rangle\langle\psi_P|1\rangle}{Z(\beta, h_A, h_B)(\Gamma z_1 z_2)^{\frac{1}{2}}}$$

$$\times (1 + \Gamma z_1 + \Gamma z_2 + z_1 z_2) + \text{H.c.} \quad\text{(A2)}$$

Therefore, we get the probe coherence L as a function of time as

$$L(t) = \frac{\hbar^2}{4}\left|\langle\sigma_x^P(t)\rangle + i\langle\sigma_y^P(t)\rangle\right|^2$$

$$= \frac{\hbar^2|\langle 1|\psi_P\rangle\langle\psi_P|0\rangle|^2}{Z^2(\beta, h_A, h_B)(\Gamma z_1^* z_2^*)}|1 + \Gamma z_1^* + \Gamma z_2^* + z_1^* z_2^*|^2$$

$$= \mathcal{C}|f(z_1, z_2)|^2, \quad\text{(A3)}$$

where $\mathcal{C} = \frac{\hbar^2|\langle 1|\psi_P\rangle\langle\psi_P|0\rangle|^2}{Z^2(\beta, h_A, h_B)(\Gamma z_1^* z_2^*)}$, and $f(z_1, z_2) = 1 + \Gamma z_1 + \Gamma z_2 + z_1 z_2$ is a bivariate LY polynomial. Hence the derivation of Eq. (7) is complete.

APPENDIX B: SAMPLING OF THE COAMOEBA: METHODOLOGY

Since, at points where the LY polynomial $|f(z_1, z_2)|^2 = 0$, the arguments of the variables represent points of the coamoeba, Eq. (9b) results in straight lines in the coamoeba

plane, with slope λ_B/λ_A, parametrized by t. As the time t elapses, a point traverses the coamoeba plane along a straight line at velocity $(4\lambda_A/\hbar, 4\lambda_B/\hbar)$. The spin coherence $L(t)$ of Eq. (7) vanishes whenever $(\theta_1(t), \theta_2(t))$ coincides with the corresponding point(s) on the coamoeba.

As an example, we plot in Fig. 6 $L(t)$ vs t, along with the parametric lines $(\theta_1(t), \theta_2(t))$ for the case $\lambda_A = J/4$, $\lambda_B = mJ/4$, $\beta = 0.5$, and $h_A = h_B = 0$, for the cases $m = 1$ and $\frac{1}{3}$. We see that $L(t)$ vanishes whenever the line $(\theta_1(t), \theta_2(t))$ intersects the coamoeba boundary. For the case $m = 1$ [Fig. 6(b)], the line only intersects the coamoeba boundary twice before it repeats after a period of $2\pi\frac{\hbar}{J}$. For $m = \frac{1}{3}$ [Fig. 6(d)], the line starts from the origin as segment A where it intersects the coamoeba once, then continues as segment B, intersecting the coamoeba twice, and finally as segment C, where it intersects the coamoeba one more time before it repeats the segments A, B, and C after a period of $6\pi\frac{\hbar}{J}$. Thus, an experimental procedure to sample a coamoeba can be done as follows. A two-spin system is prepared in a heat bath of temperature $1/\beta$, and coherence $L(t)$ of a quantum probe coupled to the system is measured. We then record the times when $L(t)$ vanishes. This gives a sequence, say, $t_1, t_2, t_3, \ldots$. By Eq. (9b), this will form a collection of points on the torus. As explained above, these mark the intersection points of the line with the coamoeba. As long as $m = \frac{\lambda_B}{\lambda_A}$ is not rational (which, in an experimental situation, is most likely the case), we can eventually collect enough points to form the shape of the coamoeba. Figure 7 demonstrates this for the ferromagnetic case $J > 0$ with t running in the interval $0 \leqslant t \leqslant 100\hbar/J$. The antiferromagnetic case is shown in Fig. 8, where t is $0 \leqslant t \leqslant 500\hbar/|J|$. In our case, m is irrational and equals to J_{PB}/J_{PA}, whose values are listed in Fig. 3(b).

APPENDIX C: EXPERIMENTS FOR $h_A = h_B = 0$

1. Preparation via probe

By setting $h_A = h_B = 0$ in Eq. (14), we get the target state

$$\rho^{\Delta}(0) = \cosh(\beta J)I_x^P + \sinh(\beta J)4I_x^P I_z^A I_z^B. \quad\text{(C1)}$$

Here we have dropped the proportionality factor of $1/Z(\beta, 0, 0)$. To prepare this, we start with the NMR thermal deviation state $\rho_{\text{th}}^{\Delta}(0)$ as mentioned in the main text and
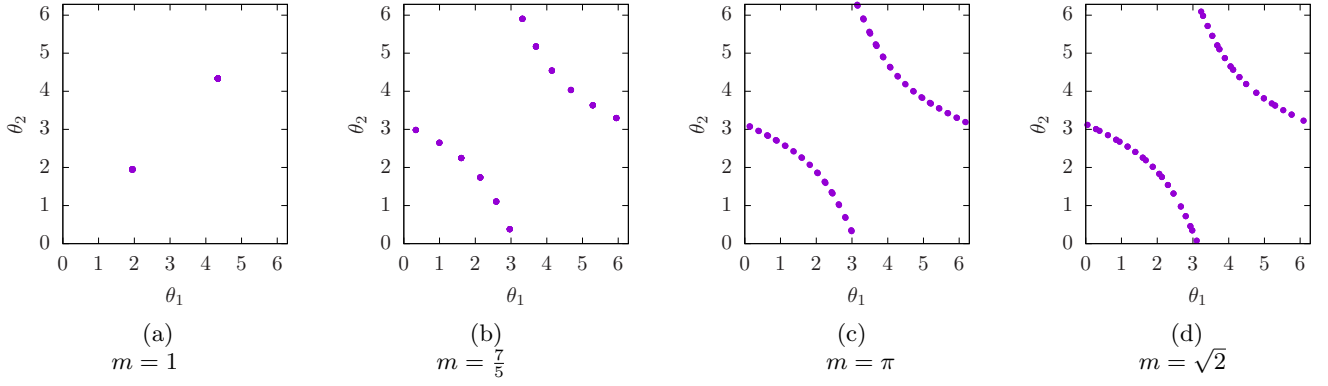
FIG. 7. Physical sampling of a coamoeba in the ferromagnetic case, $J > 0$, with $\lambda_A = J/4$, $\lambda_B = mJ/4$, and $\beta = 0.5$ for various m. The points are obtained by recording the times where $L(t)$ vanishes in the interval $0 \leqslant t \leqslant 100\hbar/J$.

proceed:

$$
\begin{aligned}
I_z^P \xrightarrow{(\pi/2)_y^P} I_x^P \xrightarrow{\tau} & \cos(\pi J_{PA}\tau)\cos(\pi J_{PB}\tau)I_x^P \\
& + \cos(\pi J_{PA}\tau)\sin(\pi J_{PB}\tau)2I_y^P I_z^B \\
& + \sin(\pi J_{PA}\tau)\cos(\pi J_{PB}\tau)2I_y^P I_z^A \\
& - \sin(\pi J_{PA}\tau)\sin(\pi J_{PB}\tau)4I_x^P I_z^A I_z^B \\
\downarrow (\pi/2)_y^P & - \text{grad.} - (\pi/2)_{-y}^P \\
\times \quad & \cos(\pi J_{PA}\tau)\cos(\pi J_{PB}\tau)I_x^P \\
& - \sin(\pi J_{PA}\tau)\sin(\pi J_{PB}\tau)4I_x^P I_z^A I_z^B.
\end{aligned}
\tag{C2}
$$

Thus the target state is achieved by applying pulses on the probe alone considering the system to be inaccessible. Here, by τ we meant free evolution under H_{eff} (given in the main text) and "grad." represents a pulsed filed gradient pulse along the z direction. In particular, the prepared state of Eq. (C2) equals the target state of Eq. (C1) (apart from trivial proportionality factors) when

$$
\frac{\cos(\pi(J_{PA}+J_{PB})\tau)}{\cos(\pi(J_{PA}-J_{PB})\tau)} = e^{2\beta J}.
\tag{C3}
$$

Therefore for any value of βJ, we can find the corresponding τ satisfying the above equation. Setting that delay time τ in
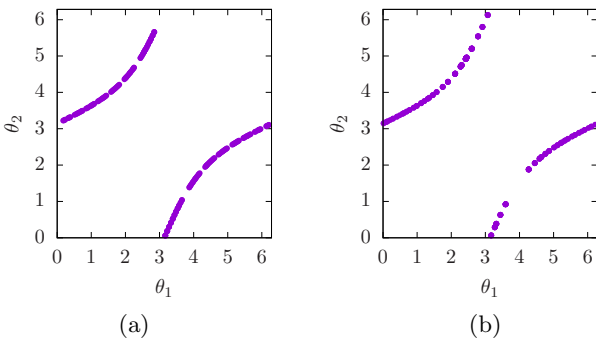

FIG. 8. Physical sampling of a coamoeba in the antiferromagnetic case, $J < 0$, where $\lambda_A = -J/4$, $\lambda_B = -mJ/4$, and $\beta = 0.5$ for (a) $m = \pi$ and (b) $m = \sqrt{2}$. The points are obtained by recording the times where $L(t)$ vanishes in the interval $0 \leqslant t \leqslant 500\hbar/|J|$.

the pulse sequence, the initial state can be readily prepared. For example, we prepare the state for $\beta J = 1/2$ by setting $\tau = 8.764\,648\,4$ ms. In this value of τ, the fidelity between Eqs. (C1) and (C2) becomes 0.99. On the other hand, to initiate the state for $\beta J = -1/2$, we set $\tau = 9.013\,671\,9$ ms in which case the respective fidelity is ≈ 1.

2. Analysis

To sample the coamoeba we initiate the system as mentioned above both for ferromagnetic ($\beta J = 1/2$) and antiferromagnetic ($\beta J = -1/2$) cases. After the initiation, as mentioned in the main text, we just need to let it evolve under its NMR internal effective Hamiltonian H_{eff} (the form is given in the main text). By direct computation, we get

$$
\begin{aligned}
\langle \sigma_x^P(t) \rangle = \text{tr}\big[& \sigma_x^P e^{-iH_{\text{eff}}t/\hbar}\big(\cosh(\beta J)I_x^P \\
& + \sinh(\beta J)4I_x^P I_z^A I_z^B\big)e^{iH_{\text{eff}}t/\hbar}\big] \\
\propto \{ & e^{\beta J}\cos[\pi(J_{PA}+J_{PB})t] \\
& + e^{-\beta J}\cos[\pi(J_{PA}-J_{PB})t]\},
\end{aligned}
\tag{C4}
$$

and

$$
\begin{aligned}
\langle \sigma_y^P(t) \rangle = \text{tr}\big[& \sigma_y^P e^{-iH_{\text{eff}}t/\hbar}\big(\cosh(\beta J)I_x^P \\
& + \sinh(\beta J)4I_x^P I_z^A I_z^B\big)e^{iH_{\text{eff}}t/\hbar}\big] = 0.
\end{aligned}
\tag{C5}
$$

As $\langle \sigma_y^P(t) \rangle$ is zero throughout, we just need to find the time points where $\langle \sigma_x^P(t) \rangle$ vanishes. In Fig. 9, we plot the real part of direct NMR FID on top of the predicted FID by analytical expression of Eq (C4) and observe they match really well. (To correct the initial phase error due to electronic switching time, etc., we have performed a zeroth-order phase correction on the data). Experimentally observed time points, where the coherence vanishes, are noted and mapped to the coamoeba torus via Eq. (9b) of the main text.

APPENDIX D: EXPERIMENTS FOR $h_A, h_B \neq 0$—PREPARATION VIA PROBE

To initialize the system at any arbitrary nonzero value of h_A and h_B, the full state mentioned in Eq. (14) becomes our target. Following the sequences of pulses given in Fig. 5(a), we achieve this preparation. Here we prove how the target is achieved by the pulse sequence of Fig. 5(a), starting from
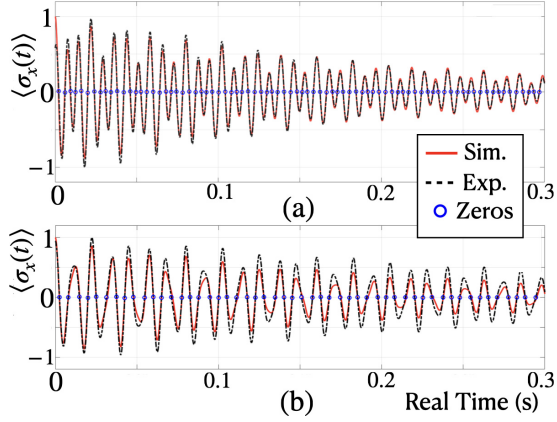
FIG. 9. (a) Simulated and experimental FID for $\beta J = 1/2$. (b) Same for $\beta J = -1/2$. Zeros of FID are marked with circles.

thermal equilibrium:

$$
\begin{aligned}
I_z^P &\xrightarrow{\theta_y^1} \cos(\theta^1)I_z^P + \sin(\theta^1)I_x^P \xrightarrow{\theta_{-x}^2} \cos(\theta^1)\cos(\theta^2)I_z^P \\
&+ \cos(\theta^1)\sin(\theta^2)I_y^P + \sin(\theta^1)I_x^P \\
&\downarrow \tau \\
&\times \cos(\theta^1)\cos(\theta^2)I_z^P + \cos(\theta^1)\sin(\theta^2)\big[\cos(\pi J_{PA}\tau) \\
&\times \cos(\pi J_{PB}\tau)I_y^P - \cos(\pi J_{PA}\tau)\sin(\pi J_{PB}\tau)2I_x^P I_z^B \\
&- \sin(\pi J_{PA}\tau)\cos(\pi J_{PB}\tau)2I_x^P I_z^A - \sin(\pi J_{PA}\tau) \\
&\times \sin(\pi J_{PB}\tau)4I_y^P I_z^A I_z^B\big] + \sin(\theta^1)\big[\cos(\pi J_{PA}\tau) \\
&\times \cos(\pi J_{PB}\tau)I_x^P + \cos(\pi J_{PA}\tau)\sin(\pi J_{PB}\tau)2I_y^P I_z^B \\
&+ \sin(\pi J_{PA}\tau)\cos(\pi J_{PB}\tau)2I_y^P I_z^A - \sin(\pi J_{PA}\tau) \\
&\times \sin(\pi J_{PB}\tau)4I_x^P I_z^A I_z^B\big] \\
&\downarrow (\pi/2)_y^P - \text{grad.} - (\pi/2)_{-y}^P \\
&\times [\sin(\theta^1)\cos(\pi J_{PA}\tau)\cos(\pi J_{PB}\tau)]I_x^P \\
&+ [-\cos(\theta^1)\sin(\theta^2)\sin(\pi J_{PA}\tau)\cos(\pi J_{PB}\tau)]2I_x^P I_z^A \\
&\times [-\cos(\theta^1)\sin(\theta^2)\cos(\pi J_{PA}\tau)\sin(\pi J_{PB}\tau)]2I_x^P I_z^B \\
&+ [-\sin(\theta^1)\sin(\pi J_{PA}\tau)\sin(\pi J_{PB}\tau)]4I_x^P I_z^A I_z^B. \quad \text{(D1)}
\end{aligned}
$$

Comparing this prepared state with the target state of Eq. (14), we note that to prepare for a given value of $\{\beta h_A, \beta h_B, \beta J\}$, we need to find corresponding values of free parameters $\{\theta^1, \theta^2, \tau\}$ from the below four equations:

$$C_a = [\sin(\theta^1)\cos(\pi J_{PA}\tau)\cos(\pi J_{PB}\tau)], \quad \text{(D2a)}$$

$$C_b = [-\cos(\theta^1)\sin(\theta^2)\sin(\pi J_{PA}\tau)\cos(\pi J_{PB}\tau)], \quad \text{(D2b)}$$

$$C_c = [-\cos(\theta^1)\sin(\theta^2)\cos(\pi J_{PA}\tau)\sin(\pi J_{PB}\tau)], \quad \text{(D2c)}$$

$$C_d = [-\sin(\theta^1)\sin(\pi J_{PA}\tau)\sin(\pi J_{PB}\tau)]. \quad \text{(D2d)}$$

Therefore it boils down to a three-parameter estimation problem, given a set of four equations. In particular, if we denote right-hand sides of Eqs. (D2a), (D2b), (D2c), and (D2d) as $\{c_a, c_b, c_c, c_d\}$, respectively, then we can define the optimization problem as

Optimize for $\{\theta^1, \theta^2, \tau\}$ such that

$$f = |\vec{C} - \vec{c}| = \sum_{i=\{a,b,c,d\}} |C_i - c_i| \text{ is minimized.} \quad \text{(D3)}$$

Any available optimization algorithm can be employed to minimize f. For example, we have used the genetic algorithm. Of course, as the system gets larger the optimization problem will become difficult unless the system possesses some symmetry. However, our method allows us to reduce this optimization problem into two optimization problems with lesser complexity. To explain how that can be done we compute $\langle\sigma_x^P(t)\rangle$ and $\langle\sigma_y^P(t)\rangle$ as the state of Eq. (14) evolves under $\mathcal{U}(t) = \exp(-iH_{\text{eff}}t/\hbar)$:

$$
\begin{aligned}
\langle\sigma_x^P(t)\rangle &= \text{tr}[\mathcal{U}\rho_\Delta(0)\mathcal{U}^\dagger\sigma_x] \\
&= C_a \cos(\pi J_{PA}t)\cos(\pi J_{PB}t) \\
&\quad - C_d \sin(\pi J_{PA}t)\sin(\pi J_{PB}t), \quad \text{(D4a)} \\
\langle\sigma_y^P(t)\rangle &= \text{tr}[\mathcal{U}\rho_\Delta(0)\mathcal{U}^\dagger\sigma_y] \\
&= C_b \sin(\pi J_{PA}t)\cos(\pi J_{PB}t) \\
&\quad + C_c \cos(\pi J_{PA}t)\sin(\pi J_{PB}t). \quad \text{(D4b)}
\end{aligned}
$$

From Eqs. (D4a) and (D4b), we note that only c_a and c_d contribute in the measurement of $\langle\sigma_x^P(t)\rangle$ while c_b and c_c terms contribute in $\langle\sigma_y^P(t)\rangle$ measurement. This mutual exclusivity can be exploited to prepare Eq. (14) via optimizing for first and last terms alone without caring for the other two terms and measuring $\langle\sigma_x^P(t)\rangle$. Then, by the same logic, we optimize only for the second and third term of Eq. (14) and measure $\langle\sigma_y^P(t)\rangle$.

As mentioned in the main text, we perform our experiments at two nonzero values of h_A and h_B, namely $\beta J = 1/2$, $\beta h_A = \beta h_B = 0.1$, and $\beta J = 1/2$, $\beta h_A = -\beta h_B = 0.1$. For each of these cases, we perform two sets of experiments by extracting $\langle\sigma_x^P(t)\rangle$ and $\langle\sigma_y^P(t)\rangle$ separately to demonstrate the before-mentioned optimization splitting. Using the optimized values, the pulse sequence of Fig. 5(b) is employed for state initialization. After initialization is achieved, $\langle\sigma_x^P(t)\rangle$ and $\langle\sigma_y^P(t)\rangle$ are recorded as the NMR register evolves freely under H_{eff} (the form is given in the main text). After zeroth-order phase correction on the experimental data, interpolated signals are plotted in Figs. 5(g) and 5(h). Their zero points (marked by circles) are then mapped to the 2-torus by Eq. (9b).

[1] C.-N. Yang and T. D. Lee, Statistical theory of equations of state and phase transitions. 1. Theory of condensation, Phys. Rev. **87**, 404 (1952).

[2] T. D. Lee and C.-N. Yang, Statistical theory of equations of state and phase transitions. 2. Lattice gas and Ising model, Phys. Rev. **87**, 410 (1952).

[3] W. Ning, R.-H. Zheng, J.-H. Lü, F. Wu, Z.-B. Yang, and S.-B. Zheng, Experimental observation of spontaneous symmetry breaking in a quantum phase transition, Sci. China Phys. Mech. Astron. **67**, 220312 (2024).

[4] A. Francis, D. Zhu, C. H. Alderete, S. Johri, X. Xiao, J. K. Freericks, C. Monroe, N. M. Linke, and A. F. Kemper, Many-body thermodynamics on quantum computers via partition function zeros, Sci. Adv. **7**, eabf2447 (2021).

[5] A. Deger and C. Flindt, Determination of universal critical exponents using Lee-Yang theory, Phys. Rev. Res. **1**, 023004 (2019).

[6] K. Brandner, V. F. Maisi, J. P. Pekola, J. P. Garrahan, and C. Flindt, Experimental determination of dynamical Lee-Yang zeros, Phys. Rev. Lett. **118**, 180601 (2017).

[7] A. Deger, K. Brandner, and C. Flindt, Lee-Yang zeros and large-deviation statistics of a molecular zipper, Phys. Rev. E **97**, 012115 (2018).

[8] N. Bastid *et al.* (FOPI collaboration), First analysis of anisotropic flow with Lee-Yang zeros, Phys. Rev. C **72**, 011901 (2005).

[9] P. Arndt, S. Dahmen, and H. Hinrichsen, Directed percolation, fractal roots and the Lee-Yang theorem, Physica A **295**, 128 (2001).

[10] M. Krasnytska, B. Berche, Y. Holovatch, and R. Kenna, Violation of Lee-Yang circle theorem for Ising phase transitions on complex networks, Europhys. Lett. **111**, 60009 (2015).

[11] M. Krasnytska, B. Berche, Y. Holovatch, and R. Kenna, Partition function zeros for the Ising model on complete graphs and on annealed scale-free networks, J. Phys. A **49**, 135001 (2016).

[12] J. Lee, Exact partition function zeros of the Wako-Saitô-Muñoz-Eaton protein model, Phys. Rev. Lett. **110**, 248101 (2013).

[13] J. Lee, Exact partition function zeros of the Wako-Saitô-Muñoz-Eaton β hairpin model, Phys. Rev. E **88**, 022710 (2013).

[14] M. Heyl, A. Polkovnikov, and S. Kehrein, Dynamical quantum phase transitions in the transverse-field Ising model, Phys. Rev. Lett. **110**, 135704 (2013).

[15] C. Flindt and J. P. Garrahan, Trajectory phase transitions, Lee-Yang zeros, and high-order cumulants in full counting statistics, Phys. Rev. Lett. **110**, 050601 (2013).

[16] R. Dorner, S. R. Clark, L. Heaney, R. Fazio, J. Goold, and V. Vedral, Extracting quantum work statistics and fluctuation theorems by single-qubit interferometry, Phys. Rev. Lett. **110**, 230601 (2013).

[17] L. Mazzola, G. De Chiara, and M. Paternostro, Measuring the characteristic function of the work distribution, Phys. Rev. Lett. **110**, 230602 (2013).

[18] B.-B. Wei, S.-W. Chen, H.-C. Po, and R.-B. Liu, Phase transitions in the complex plane of physical parameters, Sci. Rep. **4**, 5202 (2014).

[19] B.-B. Wei and R.-B. Liu, Lee-Yang zeros and critical times in decoherence of a probe spin coupled to a bath, Phys. Rev. Lett. **109**, 185701 (2012).

[20] X. Peng, H. Zhou, B.-B. Wei, J. Cui, J. Du, and R.-B. Liu, Experimental observation of Lee-Yang zeros, Phys. Rev. Lett. **114**, 010601 (2015).

[21] J. Kollár, Which are the simplest algebraic varieties? Bull. Am. Math. Soc. **38**, 409 (2001).

[22] I. M. Gelfand, M. M. Kapranov, and A. V. Zelevinsky, *Discriminants, Resultants, and Multidimensional Determinants* (Birkhäuser, Boston, 1994).

[23] O. Viro, What is an amoeba? Not. Am. Math. Soc. **49**, 916 (2002).

[24] B. Feng, Y.-H. He, K. D. Kennaway, and C. Vafa, Dimer models from mirror symmetry and quivering amoebae, Adv. Theor. Math. Phys. **12**, 489 (2008).

[25] M. Nisse and F. Sottile, The phase limit set of a variety, Algebra Number Theory **7**, 339 (2013).

[26] M. Nisse and F. Sottile, Non-Archimedean coamoebae, Contemp. Math. **605**, 73 (2013).

[27] M. Nisse and M. Passare, Amoebas and coamoebas of linear spaces, in *Analysis Meets Geometry: The Mikael Passare Memorial Volume* (Springer, New York, 2017), pp. 63–80.

[28] T. Sadykov and T. Zhukov, http://amoebas.ru/, accessed on 6 October 2023.

[29] M. A. Nielsen and I. L. Chuang, *Quantum Computation and Quantum Information* (Cambridge University Press, New York, 2010).

[30] J. Cavanagh, W. J. Fairbrother, A. G. Palmer III, and N. J. Skelton, *Protein NMR Spectroscopy: Principles and Practice* (Academic Press, New York, 1996).

[31] M. H. Levitt, *Spin Dynamics: Basics of Nuclear Magnetic Resonance* (Wiley, New York, 2013).

[32] E. Fukushima, *Experimental Pulse NMR: A Nuts and Bolts Approach* (CRC Press, Boca Raton, FL, 2018).